Annals of Biomedical Engineering, Vol. 25, pp. 460–469, 1997
Printed in the USA.

0090–6964/97 $10.50 + .00

Alteration of Hemodynamics in Aneurysm Models by Stenting: Influence of Stent Porosity

BARUCH B. LIEBER,*† ALFRED P. STANCAMPIANO,* and AJAY K. WAKHLOO†

*Department of Mechanical and Aerospace Engineering and †Department of Neurosurgery, State University of New York at Buffalo, Buffalo, NY

Abstract—Recent developments in minimally invasive approach to cerebrovascular diseases include the placement of stents in arteries for treatment of aneurysms. Preliminary clinical observations and experimental studies have shown that intravascular stents traversing the orifice may lead to thrombosis and subsequent occlusion of the aneurysm. The alterations in vessel local hemodynamics due to the introduction of a stent are not yet well understood. We investigated changes in local hemodynamics resulting from stent implantation. Pulsatile flow patterns in an experimental flow apparatus were visualized using laser-induced fluorescence of rhodamine dye. The test cells were constructed in a rectangular shape to facilitate an undisturbed longitudinal view of flow patterns in parent vessel and aneurysm models with and without porous stents. Woven nitinol stents of various porosities (76%, 80%, 82%, and 85%) were investigated. The selected fluid dynamic similarity parameters (Reynolds and Womersley numbers) represented conditions usually found in high-flow, larger arteries in humans (such as the carotid artery) and low-flow, smaller arteries (such as the vertebral artery). The mean Reynolds number for the larger arteries was 180, with maximum/minimum values of 490/−30 and the Womersley number was 5.3. The mean Reynolds number for the smaller arteries was 90, with maximum/minimum values of 230/2, and the Womersley number was 2.7. For the larger arteries modeled, placement of a stent of the lowest porosity across the aneurysm orifice resulted in reduction of aneurysmal vortex speed and decreased interaction with parent vessel flow. For smaller arteries, a stent of the same porosity led to a substantial reduction of parent vessel/aneurysmal flow interaction and the appearance of a nonrecirculating crescent of fluid rich in rhodamine dye in the aneurysm dome. Our results can help explain *in vivo* thrombus formation within an aneurysm after placement of a stent that is compatible with local hemodynamics.

Keywords—Aneurysm, Cerebrovascular, Intravascular stent, Hemodynamics, Laser-induced fluorescence.

INTRODUCTION

Stroke is the most common, life-threatening neurological disease and the third largest cause of death in the United States (19). In 1994, approximately 500,000 Americans suffered a stroke, and there are more than 3 million stroke survivors in this country with varying degrees of disability (5). In 1994, 154,000 deaths were attributed to stroke in the United States. One-fourth of the deaths from cerebrovascular disease in the United States arise from hemorrhage and stroke associated with rupture of intracranial arterial aneurysms. The incidence of intracranial aneurysms in the general population has been reported as between 1.5 and 8.0% (3). Based on autopsy studies, 5 million individuals in North America are estimated to harbor an intracranial aneurysm. Approximately 28,000 patients suffer from an acute intracranial hemorrhage each year (7).

Currently, the standard approach for the treatment of intracranial aneurysms is craniotomy, with clipping of the aneurysm neck to exclude it from circulation. However, this is a highly cost-intensive approach and may add to a higher morbidity resulting from associated vasospasm and brain edema. Currently applied endovascular techniques include metal microcoils that are inserted into the aneurysm via microcatheters. The coils reduce the blood circulation within the aneurysmal pouch, which leads to thrombosis. However, there are associated risks of coil protrusion into the parent vessel and a risk of aneurysm rupture (16). In addition, coil-treated aneurysms may remain incompletely occluded with persisting risk of rupture. Despite advancements in both approaches, there are still many aneurysms that both surgical and currently available minimally invasive endovascular approaches cannot effectively cure.

Recently, intravascular porous tubular-shaped stents are being considered for the endovascular treatment of intracranial aneurysms. Stents may indirectly promote thrombosis of the aneurysmal pouch by altering blood flow within, thereby preventing further deleterious effects of aneurysm growth and rupture.

Preliminary experimental studies and clinical case re-

Acknowledgment—We are thankful to Boston Scientific Corporation for providing us with the stents for this study and to Debra Zimmer for editorial assistance. This work was supported by the State University of New York at Buffalo under the Ralph Hochstetter Medical Research Fund in honor of Dr. Henry C. and Berta H. Buswell, and by the Whitaker Foundation under Grant 95-0028.

Address correspondence to Baruch B. Lieber, Department of Mechanical and Aerospace Engineering, State University of New York at Buffalo, 324 Jarvis Hall, Buffalo, NY 14260, U.S.A.

(Received 22Jul96, Revised 24Sep96, Revised, Accepted 10Oct96)

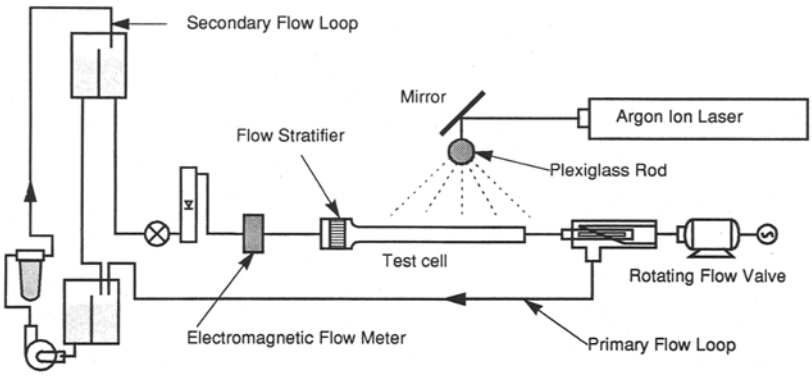

FIGURE 1. Experimental apparatus shows primary and secondary flow loops. The test cell is located in the center immediately after the flow stratifier and upstream of the rotating flow valve. The laser beam is refracted through the plexiglass rod forming a sheet of laser light over the test cell.

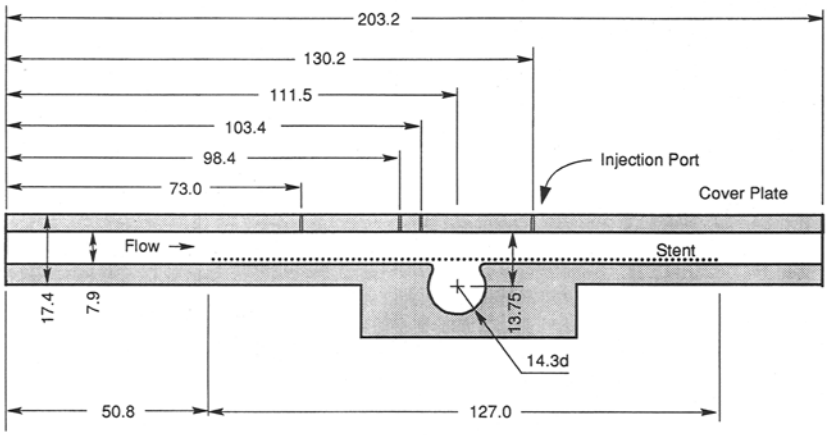

FIGURE 2. Schematic diagram of the test section (all dimensions are in mm). The radius of curvature of the aneurysm lips is 2.4 mm.

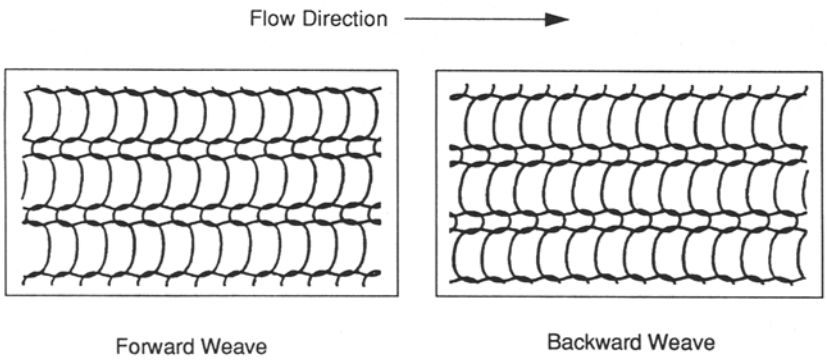

FIGURE 3. Magnified stent structure showing pore geometry with forward and backward weave directions relative to the flow.

ports show that stents are able to permanently occlude side wall aneurysms of the carotid artery (9,17). After thrombosis of the aneurysmal pouch, the side of the stent that faces the flow in the parent vessel is covered by a thin layer of neointima that allows the reestablishment of physiological flow. Complex hemodynamic mechanisms promote aneurysm thrombosis (17), but are not yet well understood and should be further investigated to improve stent technology.

Previous *in vivo* experimental studies show that stent geometry (filament diameter, and porosity), mechanical properties, material properties (alloy, surface charge, and surface tension), and biocompatibility are likely to be most important for immediate and long-term successful results (10,18). Among these parameters, the porosity of a stent is of particular importance because high resistance to flow through the stent pores into the aneurysmal pouch, combined with a low-driving pressure gradient, may prevent the recirculation of flow into the aneurysm, thereby inducing flow stasis in the pouch that promotes rapid thrombosis. This study investigates flow patterns in side wall aneurysm models under two distinctly different hemody-

namic conditions. The influence of stenting and the effect of variations in stent porosity on the flow domain were explored.

METHODS

Flow Apparatus

A recirculating flow apparatus with a constant pressure head and two reservoirs was constructed. The flow apparatus consisted of primary and secondary flow loops (Fig. 1). The primary loop used gravity feed with pressure head to reproduce *in vivo* flow conditions. Fluid entering the primary loop from the upper reservoir was regulated by a control valve and rotameter device before entering the flow stratifier. The test cell was positioned upstream of a rotating flow valve, and the fluid from this valve was discharged into the lower reservoir. An overflow on the left side of the upper reservoir maintained a constant pressure head in the right side of the system after a steady state was reached. To complete the loop, clear vinyl tubing of 12.7 mm. i.d. was used between system components.

A flow stratifier consisting of a baffle, a bundle of straws, and a contraction was located immediately upstream of the test cell. As fluid from the tube proceeded, the baffle reduced the flow velocity and jet effect, and the straw bundle the turbulence. Fine mesh screens were placed over the passages to and from the straw bundle to suppress further free-stream turbulence (8). Immediately after the straw bundle, the 4:1 cross-sectional area contraction reduced the cross-section of the flow tube to that of the test cell, which was 1.01 cm^2. The exit of the contraction was sized so it would fit snugly into the test cell. The contraction further reduced turbulent eddies by stretching them.

The secondary flow loop of the apparatus pumped fluid from the lower to upper reservoir and used an electric motor (1/25 horsepower) to turn a magnetic-drive coupled pump. The pump was mounted on a separate base and placed on rubber pads to prevent vibrations from reaching the test section of the flow apparatus. Fluid that entered the lower reservoir from the primary loop contained rhodamine dye. An active charcoal filter located between the pump and the upper reservoir prevented the access accumulation of dye in this working fluid.

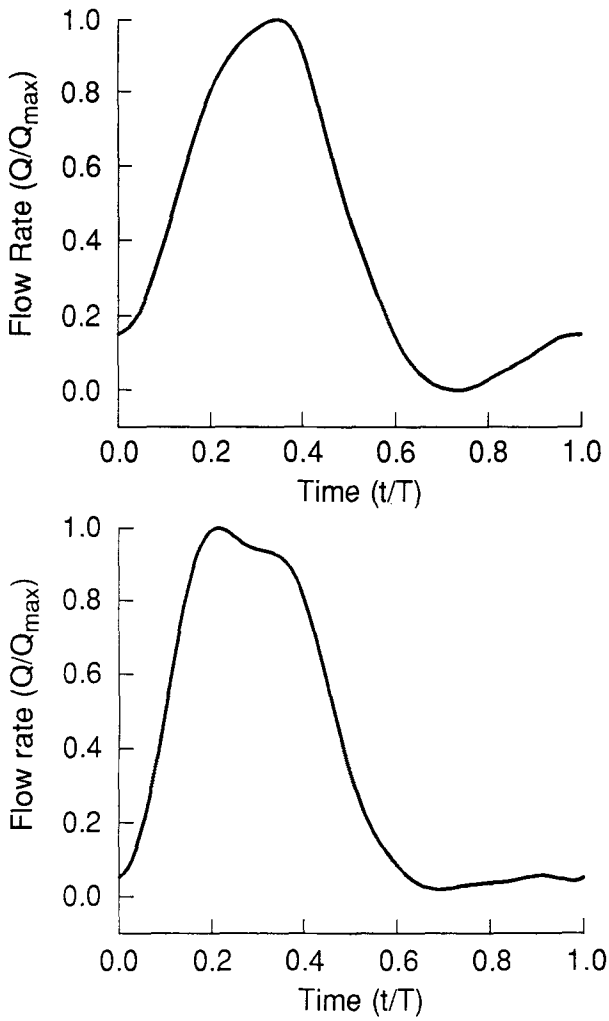

FIGURE 4. Pulsatile waveform for the two different hemodynamic parameters studied. Top waveform for Womersley number of 5.3 (high hemodynamic setting) and bottom waveform for Womersley number of 2.7 (low hemodynamic setting).

Test Cells

The aneurysm geometry and specifications of the test cell design are given in Fig. 2. Each test cell was composed of nondistensible walls with a rectangular cross-section. The first 4.76 mm of the inner channel of each test cell was enlarged by 0.80 mm to produce a flush junction

FIGURE 5. Flow patterns in stented versus nonstented (ns) aneurysms. Arrow in panel A indicates bulk flow direction. Left column shows flow patterns during early systole (t = 0.135T), and right column shows flow patterns during diastole (t = 0.755T). (A and B) Fast hemodynamics in a nonstented aneurysm (α = 5.3). The arrow in panel B indicates converging streaklines of parent vessel flow reversal and clockwise vortical motion into the aneurysm. (C and D) Flow patterns in an aneurysm with a stent of 76% porosity; stent location is indicated by the arrow in panel C [mesh density (md) = 50 pores/cm^2 and filament diameter (fd) = 150 μm] for same hemodynamic conditions. Notice the breakup of the vortex during systole and the reduced aneurysmal vortex interaction with the parent vessel during diastole. (E and F) Flow patterns in the nonstented aneurysm for slow hemodynamic conditions (α = 2.7). Interaction of aneurysmal vortex with parent vessel is reduced, compared with the faster conditions. (G and H) Flow patterns in the stented model (76% porosity) for the same hemodynamic setting. During systole, there is no vortex formation in the aneurysm. Delayed vortex formation is visible during diastole. A crescent of dye at the aneurysm dome is not participating in mass exchange with the flow outside it. Momentum exchange is limited to oscillating the crescent back and forth.

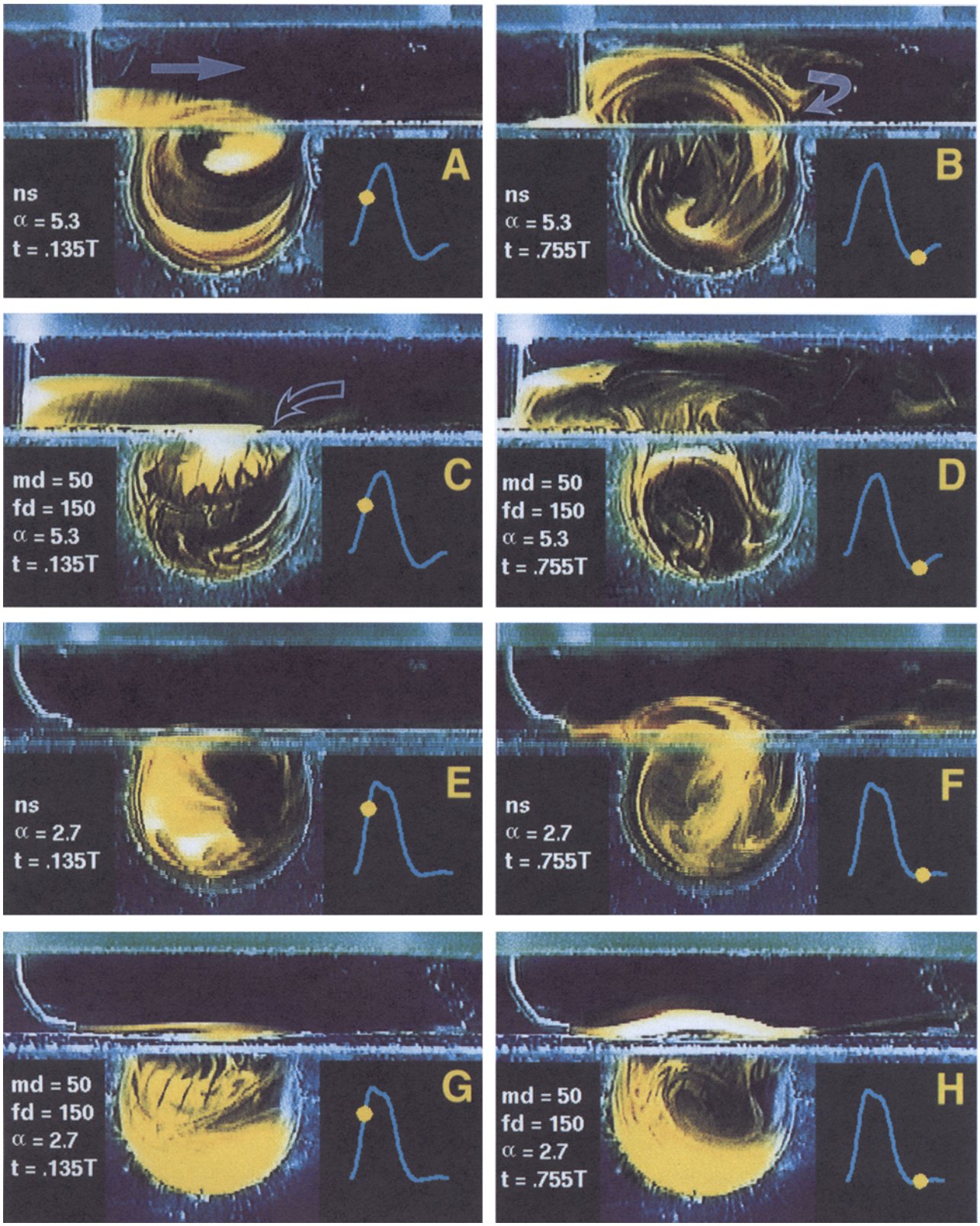
A
ns
α = 5.3
t = .135T
B
ns
α = 5.3
t = .755T
C
md = 50
fd = 150
α = 5.3
t = .135T
D
md = 50
fd = 150
α = 5.3
t = .755T
E
ns
α = 2.7
t = .135T
F
ns
α = 2.7
t = .755T
G
md = 50
fd = 150
α = 2.7
t = .135T
H
md = 50
fd = 150
α = 2.7
t = .755T

between the contraction and test cell for smooth transition of flow from one component to the next without tripping. A total of six test cells were constructed, with aneurysms milled into the base before stent placement. The cross-sectional dimensions of each test cell were 1.27 cm × 0.79 cm (1.01 cm^2 cross-sectional area) with an equivalent hydraulic diameter of 0.98 cm. This design was based on 6 mm, inner diameter self expanding stents made of nitinol (Boston Scientific Corporation, Natick, MA, USA), a heat-treated alloy consisting of nickel and titanium. Thus, the test cell width was limited to the circumference of a 6 mm i.d. stent. Four 1.59 mm ports were drilled into each cover plate and filled with clear silicone rubber to prevent fluid leakage. Laser dye was injected into the flow field by a hypodermic needle passing through those silicone-filled ports.

A symmetrical aneurysm geometry was selected for machining convenience and comparison to computer simulations (1). Six different test cells were used for each hemodynamic condition. The test cells included a non-stented model and stented model with variations in the following parameters: filament diameter, mesh density, and a change in weave direction. Two different filament diameters 125 and 150 μm, and of both low mesh density (35 pores/cm^2) and high mesh density (50 pores/cm^2) were used. The thickness of the flattened stent layer was equivalent to the filament diameter, except at the filaments cross-over junctions (Fig. 3) where it was twice that of the filament diameter. Variations of filament diameter and mesh density produced four models with different porosities, defined as a percentage of metal free unit area per total unit area of the stent. The porosity of the thick filament, high mesh density stent was 76%. The thin filament, high mesh density stent had a porosity of 80%. The thick filament, low mesh density stent had a porosity of 82%, and the thin filament, low mesh density stent had a porosity of 85%. The remaining was made with stent material that had 150 μm filament diameter and a high mesh density (76% porosity), but with the weave direction backward relative to the flow (Fig. 3).

Pulse Generator Mechanism

A rotating flow valve (11,14) located between the test cell and lower reservoir produced pulsating flow mimicking the Womersley parameter and rate of blood flow through the carotid and vertebral arteries. Pulsations were produced by varying the volumetric flow, not by changing the pressure. Fluid entered the valve through an inner pipe that was rotated by a 1/25 horsepower electric motor, and exited the pipe through a long narrow slit in its side wall. This inner pipe was encased by a cylindrical sleeve cut at an angle relative to its concentric axis. The rotation of the inner pipe within the sleeve varies the exposed cross-section of the fluid exit slit. The outer sleeve can be modified to produce pulsations mimicking a pulsatile waveform similar to the cardiac cycle. The waveform was quantified by placing an electromagnetic flow probe (Gould Statham, Oxnard, CA, USA; Model SP2202) connected to a data acquisition board.

For calibration purposes, data from the flow probe was collected for 180 sec at 100 samples/sec for six different flow rates. During each data collection period, the total fluid volume was also collected and recorded. Each data file was then integrated over the collection period with the resulting values plotted against the corresponding total volumes of flow. The plot of these six data points verified linearity of the flow probes, so the linear regression was calculated to obtain the slope and y intercept for the line of calibration. Subsequent to calibration, data were collected for flow through the probe at the hemodynamic conditions selected. These records were used to calculate the flow through the probe using the regression coefficients previously obtained. The resulting flow through the probe was lowpass-filtered using a 12th order Butterworth filter to smooth the resulting final flow curve through the test section. The valve was operated at 60 rpm for a pulse duration of $T = 1$ sec for the high hemodynamic setting, and at 28.33 rpm resulting in a pulse duration of $T = 2.12$ sec for the low hemodynamic setting. The final normalized flow curves are shown in Fig. 4 for the two different hemodynamic settings.

Flow Parameters

Modeling arterial blood flow *in vitro* requires simplifying assumptions about various parameters of the flow and the vessel (such as Newtonian or non-Newtonian fluid properties and rigid or compliant walls). For blood to be considered a Newtonian fluid, a high rate of shear must prevail such that the coefficient of apparent viscosity approaches a representative constant value. This predominately occurs during systole in blood vessels larger than 0.5 mm in diameter (4). Because flow is unsteady, the dimensionless frequency parameter (or the Womersley number, or the unsteadiness parameter), α, must be considered in addition to another independent dimensionless group, such as the Reynolds number, to facilitate dynamic similitude. The Womersley number is the ratio of transient inertial forces and viscous forces that accounts for the angular frequency of the flow pulsatility.

The Newtonian working fluid used was a water/glycerin mixture of the two different mass fraction ratios to simulate two distinct hemodynamic conditions. One set of flow parameters was chosen to represent conditions found in larger arteries, such as the human carotid artery. For these high hemodynamic settings, the combined action of gravitational feed, control valve, and rotating valve was driving the flow at a Womersley number of $\alpha = 5.3$. The Reynolds number range was 490/180/–30 (maximum/

mean/minimum) based on instantaneous flow rate. The second set of flow parameters was chosen to represent conditions found in smaller arteries, such as the human vertebral artery (20). For these low hemodynamic settings, the flow was driven at a Womersley number of 2.7, and the Reynolds number range was 230/90/2. For the higher hemodynamic setting, a 1:1 mass fraction ratio was used. The resulting viscosity of this mixture is 6 cp, with a kinematic viscosity of 5.37 cs at the operating temperature of 27°C. For the lower hemodynamic setting, a 1:1.63 mass fraction ratio was used. The resulting viscosity of this mixture is 11.23 cp, with a kinematic viscosity of 9.74 cs at the same operating temperature.

Laser-Induced Fluorescence

Flow patterns in the models were visualized by laser-induced fluorescence (2,6,12). Laser-induced fluorescence was configured to produce two-dimensional, mid-cross-sectional, lengthwise images of the flow field. Flow visualization was accomplished by injecting rhodamine chloride 590 (λ = 590 nm) dye into the flow field through one of the four ports in each test cell while illuminated by laser light. Before injection, the dye was placed in a water and glycerin solution that had the same viscosity and temperature as the working fluid. A dye concentration of 10 mg/kg was infused through a microcatheter and needle using a syringe infusion pump (Harvard Apparatus 22, South Natick, MA, USA) at a rate of 3 ml/min. The 18-gauge microcatheter was ~120 cm in length with a 22 gauge × 2.0 cm needle attached to the end. The tip of the needle was filed flat, deburred to remove the angle typically present on medical grade syringe needles, and then bent to a right angle.

A 4-Watt argon ion (λ = 514.5 nm and 488.0 nm), water-cooled laser (Lexel Excel 3000) was used to produce the necessary vertical plane of laser light (Fig. 1). Initially, the laser beam was reflected off a quarter wavelength, first surface mirror placed at a 45° angle, which changed the beam's plane from horizontal to vertical. The beam was then refracted through a plexiglass rod, creating a sheet of laser light. This sheet impinged on the test cell's midplane over its entire length. The intensity of the laser was varied to help optimize dye fluorescence and thereby the quality of the video recording. By adjusting the horizontal and vertical positions of the plexiglass rod, the thickness of the laser sheet was controlled. The best spatial resolution was obtained when the laser sheet thickness was 1 mm or less.

Results were recorded using a videocamera (Sony Video Hi8 CCD Handycam camcorder operating at 30 frames/sec), with magnifying lenses in front of the camera for increased spatial resolution. The field of view for the flow recordings focused on a 3.0-cm section of the test cell. Each test cell was placed in the flow apparatus and videotaped under the same conditions, including Reynolds number, Womersley number, dye concentration, and point of dye injection. The video signal was connected in parallel to both the videocamera and a television screen. The video recordings were started a few cycles after dye injection was initiated, and dye structures in the field of view have reached steady state with no apparent visible changes from cycle to cycle.

The video recordings were started at approximately the same point in the pulse cycle, with each test cell so the on-screen timer could be used to compare the pulses. Visual frame by frame inspection of the video recordings showed that the dye structures were indeed repeatable from one flow cycle to the next. The test cell flow patterns were recorded twice, once with the aneurysm below the flow channel and then with the aneurysm above the flow channel, to examine the effects of gravity. A random flow cycle within each video segment was selected to obtain photographic results. Using a frame grabber, two frames within the pulse were recorded and saved as printable image files. The first frame for each sequence was acquired during the acceleration phase of systole at t = 0.135T. The second frame was acquired during mid-diastole at t = 0.755T.

RESULTS

Flow at High Hemodynamic Setting (α = 5.3, R_e = 490/180/−30).

Figure 5 (A and B) shows the results for the high hemodynamic flow patterns in the nonstented aneurysm, whereas Fig. 5C,D shows corresponding flow through the model containing the stent with 76% porosity. Bulk flow direction is from left to right, as indicated by the arrow in Fig. 5A. During early systole (acceleration), dye entered the nonstented test cell as a thick continuous streakline forming a vortex positioned between the aneurysmal sac and parent vessel, but mostly inside the aneurysm (Fig. 5A). The vortex traveled across the aneurysm orifice as systole progressed. The distal neck acted as a flow divider when the vortex encountered it, forcing fluid further down the parent vessel or into the aneurysmal pouch. The portion of the vortex that was forced into the pouch moved along the distal side wall to the aneurysm dome while continuing to circulate. As flow continued after peak systole, an influx of flow entering distally pushed the vortex toward the proximal side of the aneurysm and partially back into the parent vessel. Similar behavior of vortex ejection into the parent vessel has been reported in Ref. 13 for flow through an axisymmetric aneurysm and side wall rectangular cavity at much lower Reynolds numbers.

The remaining vortex began to circulate in the center of the sac. Small but noticeable amounts of fluid entered the

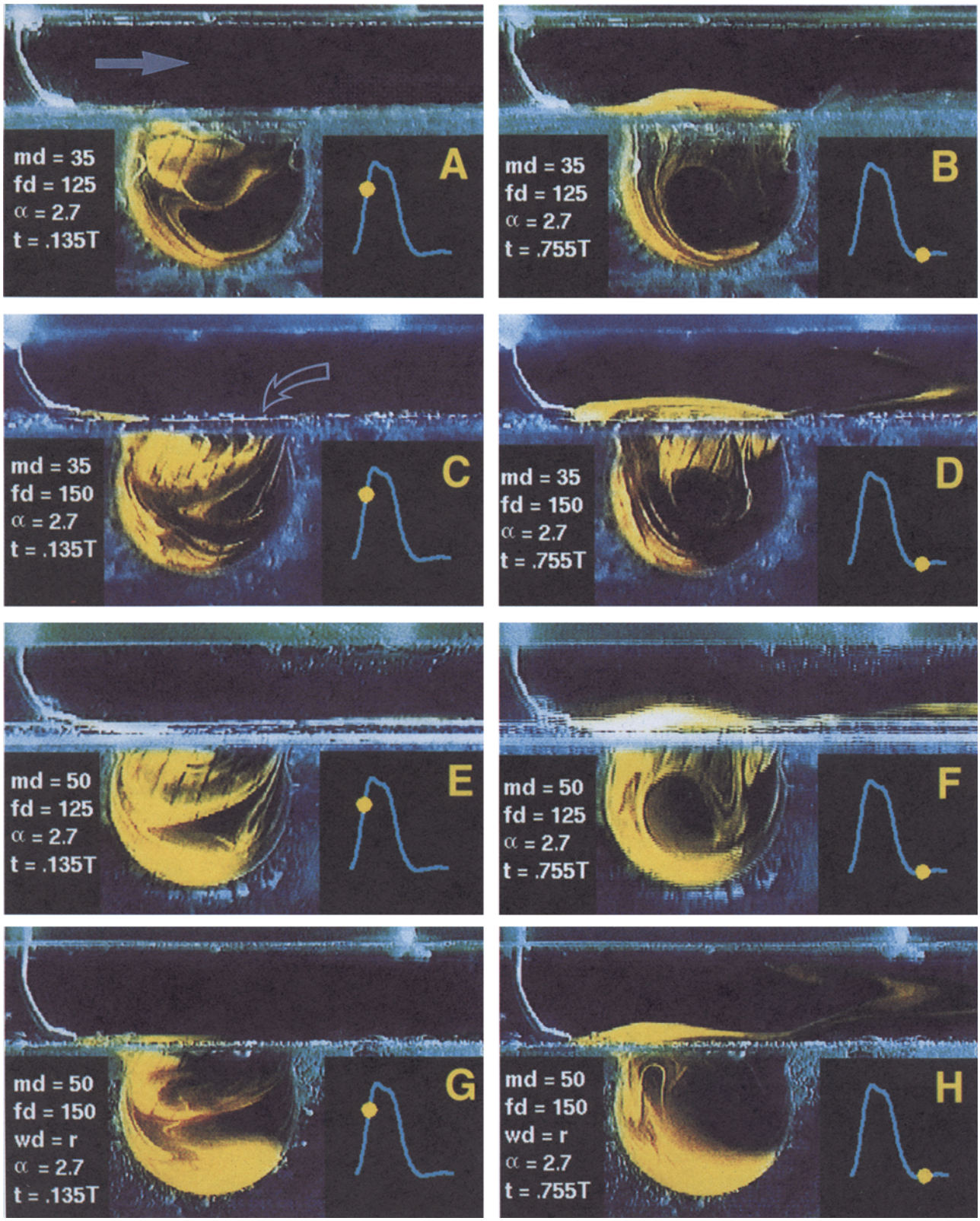

FIGURE 6. Influence of variations in stent porosity on aneurysmal flow patterns during systole and diastole. Bulk flow direction indicated by the arrow in panel A and stent layer location by the arrow in panel C. Most notable feature is the change of size of the crescent of fluid-rich dye in the aneurysm dome region. (A and B) 85% porosity stent (low mesh density and thin filament) produced the smallest crescent. (C and D) 82% porosity stent (low mesh density thick filament diameter) produced a slightly thicker crescent than the previous. (E and F) 80% porosity stent (high mesh density thin filament diameter) produced a noticeable thicker crescent than the previous two. (G and H) The thickest crescent was produced by the 76% porosity stent (high mesh density thick filament diameter). The stent shown herein was positioned with backward weave direction (wd = *r*) relative to the flow; however, these results are qualitatively indistinguishable from the forward weave direction results (Fig. 5G,H). md, mesh density; fd, filament diameter.

aneurysm distally and exited proximally, forming a path of flow along the perimeter of the aneurysm during late systole (deceleration). This point in time marked the approximate beginning of the diastolic phase (Fig. 5B). Parent vessel flow was near quiescent during diastole, and flow that had entered the aneurysm distally during the systole continued to exit the aneurysm proximally and accumulated in the parent vessel during diastole. Flow reversal in the parent vessel occurred for a short period. During this period, flow into the aneurysm near the distal neck was also fed by distal channel fluid, now moving upstream, as shown by the two streamlines converging at the distal aneurysm neck (indicated by the arrow in Fig. 5B). Flow during late systole exited the aneurysmal pouch near the upstream corner in a jet-like fashion perpendicularly to the vessel axis leading to disturbances in streamwise parent flow. Meanwhile, flow in the center of the aneurysm continued to recirculate as fluid along the perimeter fed through the distal neck was ejected through the proximal neck. Thereafter, parent vessel flow rapidly increased as systole of the next cycle was about to begin clearing away all visible streaklines. All the fluid inside the aneurysm was participating in vortical motion. There were no regions of stagnation visible in the entire field of view.

Results for flow through a stented aneurysm (stent porosity of 76%) at high hemodynamic setting are shown in Fig. 5C,D. Flow entering the stented aneurysm was forced into separate pathways through the pores (Fig. 5C, arrow indicates the location of the stent layer). It proceeded into the aneurysm between filaments in a noncircular motion hitting the quiescent fluid in the dome region of the aneurysm. Each of the cross-wise filaments acted as a path divider to the approaching flow, much like the distal aneurysmal neck in the nonstented case. A vortical motion immediately followed, with streaklines entirely contained within the aneurysmal sac. During late systole, this motion was sustained as a result of influx into the aneurysm sac distally, fed by split streaklines from the parent vessel, similar to the nonstented case but to a lesser degree. As the aneurysm vortex continued to rotate, some streaklines close to the periphery of the vortex near the proximal opening were forced through the stent pores back into the channel flow and swept by it. Fluid exchange between parent vessel and aneurysmal flow was less, compared with the nonstented case. The remaining vortex in the aneurysmal sac was forced upward and proximally along the aneurysm wall, and then its center proceeded slowly toward the dome. With the onset of diastole, flow entering the aneurysm at the distal neck was partially fed by upstream vessel flow, indicated by the split streamline located at the entry. Quiescent parent vessel flow was disturbed by the aneurysm outflow forced through the pores back into the vessel (Fig. 5D). As in the nonstented case, there were no apparent regions of stagnation, and all of the aneurysmal fluid participated in mass and momentum exchange between the aneurysmal sac and parent vessel flow during each cycle.

Flow at Low Hemodynamic Setting (α = 2.7, R_e = 230/90/2).

Figure 5E,F show flow patterns in the nonstented test cell for the low hemodynamic setting, whereas Fig. 5G,H shows flow patterns for the stented test cell, with a stent of 76% porosity. In the nonstented case, because of the slower rotation rate of aneurysm vortex, not all of the dye accumulated in the aneurysm was washed out of each cycle. Moreover, when we stopped injecting the dye, several pulse cycles were required to wash the dye completely from the aneurysm. At the onset of systole, dye streaklines traversing the aneurysmal orifice split after crossing ~60% of the orifice width. One streakline continued along the vessel, whereas the other entered the aneurysm and proceeded clockwise along the distal wall in a vortical fashion. However, the flow did not have enough momentum to wash dye-rich fluid remaining in the proximal portion of the aneurysm from the previous flow cycle into the parent vessel. As a result, two distinct regions of aneurysmal flow were apparent: slow, upward moving fluid in the proximal portion of the aneurysm entrained by the faster moving fluid distally, with mixing at the center. During diastole, the aneurysm vortex continued to rotate but, because of a quiescent period in parent vessel flow, its center moved toward the parent vessel (Fig. 5F). This motion caused the vortical streaklines to protrude into the parent vessel in a fashion similar to the higher hemodynamics case, but to a lesser degree. In addition, the faster moving central portion of the aneurysmal vortex completely entrained the slower part forcing the accumulated dye in the periphery toward the parent vessel. The aneurysmal vortex, however, did not sustain enough momentum to push the bulk of fluid rich in dye back into the parent vessel. A portion of the peripheral flow recirculated back into the aneurysm. In summary, compared with the high hemodynamic setting for the nonstented case, the flow patterns in the aneurysm were qualitatively similar; however, the lower hemodynamic setting somewhat impaired the exchange of momentum between aneurysm and parent vessel flow.

A substantially different flow field was observed in the stented aneurysm model (76% porosity) at the lower hemodynamic setting (Fig. 5G,H). One substantial difference was a stable crescent of dye that accumulated at the aneurysm dome. There was no exchange of the dye in this region and the aneurysmal flow, except around the boundary and at the tips of the crescent. The dye crescent kept oscillating back and forth around the dome region because of entrainment with vortical motion in the rest of the aneurysm during the pulse cycle. Even after we stopped

injecting dye and after several pulse cycles, the dye from this region was not washed from the aneurysm. During systole (Fig. 5G), dye traversing the aneurysm orifice was partially washed down the vessel. The remainder seeped through two-thirds of the aneurysm orifice through the stent filaments and down toward the center of the aneurysm to the dome. During late systole approaching early diastole, a slowly rotating vortex developed in the distal portion of the aneurysm outside the crescent and spanned about one-half of the aneurysm width. This vortex gave momentum to the crescent, which then moved slowly to the proximal region of the aneurysm (Fig. 5G). The upward motion of the crescent also entrained small amounts of the dye from its proximal tip back into the parent vessel flow. During diastole, the aneurysmal vortex moved toward the parent vessel and induced slight undulation of the streaklines above the stent filaments.

Variations in Stent Parameters

Results for additional test cells with variations in porosity and weave direction are presented for the low hemodynamic setting only. Flow patterns of stents with 85% porosity (Fig. 6A,B), 82% porosity (Fig. 6C,D), and 80% porosity (Fig. 6E,F) were qualitatively similar to that of the stent described in Fig. 5G,H. The size of the crescent that was formed in the aneurysm dome was effected by the porosity of the stent (Fig. 6A–F). The stent with highest porosity (85%) produced the smallest crescent of isolated fluid, with the highest oscillations in the dome region. The 82% porosity stent produced similar results with a slightly thicker crescent. The 80% porosity stent produced a thicker crescent with lower amplitude oscillations than the previous two stents; however, this crescent was not as large as that produced by the stent with the lowest porosity tested (76%). A weave reorientation in direction backward to the flow for the 76% porosity stent had no qualitative effect on the flow field around the stent (Fig. 6G,H).

DISCUSSION

Techniques for the endovascular treatment of intracerebral aneurysms have advanced significantly in the last few years. Intravascular stenting may be an alternative endovascular treatment. Detailed knowledge of hemodynamic changes in cerebral aneurysm after stenting is needed. In this investigation, flow patterns in side wall aneurysm models were studied under two distinctly different hemodynamic conditions. Self-expanding woven stents of nitinol were introduced into the flow field, and the influence on the flow domain of variations in porosity and weave direction was explored.

The most significant finding was the reduction of flow activity inside the aneurysmal pouch after stent placement across the aneurysmal orifice. Stenting reduced the streakline rotation rate within the aneurysmal pouch. The presence of the stent partially uncoupled aneurysmal flow from that of the parent vessel and reduced momentum and mass exchange between the two. Porosity of the stent in conjunction with local hemodynamics played a significant role in the uncoupling. While in the high hemodynamic setting, stents with the lowest porosity (76%) did not alter the flow velocity inside the aneurysm significantly; regions of flow stagnation were observed in the low hemodynamic setting for a stent of the same porosity. In the low hemodynamic setting, a crescent of dye in the aneurysm dome region appeared that did not participate in mass and momentum exchange with the remaining aneurysmal flow. The size of the crescent was closely related to the porosity of the stent. The best configuration was achieved with the stent of the lowest porosity (76%). The porosity of stents in this investigation was limited to that of currently available nitinol stents, which were also used in our previous animal studies (17,18).

Our results with four different stents in a low hemodynamic setting suggest that, in a high hemodynamic condition, further reduction of stent porosity is required to reduce the flow velocity sufficiently. Nonetheless, whether stagnant flow inside the aneurysm is a prerequisite to thrombus formation needs to be scrutinized by *in vivo* experiments. Simply decreasing the porosity of the stent, however, has adverse effect on the biological response of the vessel wall. Excessive neointimal response, with a risk of secondary stenosis of the artery, is seen with a higher stent metal-to-arterial tissue ratio (15). In addition, decreasing the porosity alone may reduce the flexibility of a stent, thus affecting its endovascular delivery and implantation into the tortuous cerebrovascular system. Selection of proper stent porosity for the prevailing hemodynamic condition may be accomplished by using flow visualization in concert with animal experiments.

Gravitational forces may play a role in the mixing of fluids of dissimilar densities. Dye was suspended in the same liquid as the working fluid to negate the influence of gravitational forces. To evaluate whether these forces played a role in our results, the models were studied twice, with test cells rotated 180° around the flow axis. These results showed no qualitative differences in flow patterns between aneurysms overlying or underlying the parent vessel, suggesting that gravity played a negligible role.

In the nonstented test cell, an aneurysmal vortex that formed during early systole projected into the parent vessel at diastole. In contrast, in the stented test cells, the vortex was confined to the aneurysm. Changes of vortex location, speed, and reductions of aneurysmal flow and momentum exchange with the parent vessel flow support our hypothesis that stents can favorably alter aneurysmal hemodynamics. Stent-induced flow stagnation may aid the

formation of a stable thrombus in the pouch and lead to permanent occlusion of the aneurysm.

It is interesting to speculate on the *in vivo* consequences of stent implantation for the purpose of intravascular bypass of aneurysms. The available modalities for combating aneurysms involve the exclusion of the aneurysm from the circulation by either endosaccular treatment, parent vessel occlusion, or surgical clipping. Endosaccular treatment is limited to aneurysms with narrow, well-defined orifices and ineffective for broad-based or giant aneurysms. Parent vessel occlusion is limited to cases with well-developed collateral circulation. Clipping is limited to surgical accessibility of the aneurysm. Bypassing the aneurysm with a stent in the parent artery may be used for those aneurysms that are not amenable to currently available treatment. In addition to exclusion of the aneurysm from the circulation, the stent mesh can serve as a substrate for neointimal growth, as observed in our previous animal studies, and induce remodeling of the arterial segment treated.

REFERENCES

1. Aenis, M., A. P. Stancampiano, A. K. Wakhloo, and B. B. Lieber. Modeling of flow in a straight stented and nonstented side wall aneurysm model. *J. Biomech. Eng.* 1997, in press.
2. Baker, J. K. Analysis of the turbulent plane wake using laser Doppler anemometry and laser induced fluorescence. Buffalo: State University of New York at Buffalo, M.S. Thesis, 1992.
3. Bannermann, R. M., G. B. Ingall, and C. J. Graf. The familiar occurrence of intracranial aneurysms. *Neurology* 20:283–292, 1970.
4. Chandran, K. B. Cardiovascular Biomechanics. New York: New York University Press, 1992.
5. Doyle, R. Stroke mortality in men ages 35 to 74. *Sci. Am.* 274:26, 1996.
6. Hartfield, R. J. Jr., S. D. Hollo, and J. C. McDaniel. Planar measurement technique for compressible flows using laser-induced iodine fluorescence. *AIAA J.* 31:483–490, 1993.
7. Kassell, N. F., and J. C. Torner. Epidemiology of intracranial aneurysms. *Int. Anesthesiol. Clin.* 20:13–17, 1982.
8. Loehrke, R. I., and H. M. Nagib. Control of free-stream turbulence by mean of honeycombs: a balance between suppression and generation. *J. Fluids Eng.* 98:342–353, 1976.
9. Marks, M. P., M. D. Dake, G. K. Steinberg, A. M. Norbash, and B. Lane. Stent placement for arterial and venous cerebrovascular disease: preliminary clinical experience. *Radiology* 191:441–446, 1994.
10. Palmaz, J. C. Intravascular stent: tissue-stent interactions and design considerations. *Am. J. Roentgenol.* 160:613–618, 1993.
11. Schultz-Grunow, F. Pulsating flow through pipes (original in German). *Forschung* 11:170–187, 1940 (English reference, NASA-TT-F-14881, 1973).
12. Serpenguzel, A., J. C. Swindal, R. K. Chang, and W. Acker. Two-dimensional imaging of sprays with fluorescence, lasing, and stimulated raman scattering. *Appl. Optics* 31:3543–3551, 1992.
13. Stephanoff, K. D., I. J. Sobey, and B. J. Bellhouse. On flow through furrowed channels. Part 2. Observed flow patterns. *J. Fluid Mech.* 96:27–32, 1980.
14. Stettler, J. C., and A. K. M. Fazle Hussain. On transition of pulsatile pipe flow. *J. Fluid Mech.* 170:169–197, 1986.
15. Tominaga, R., H. Harasaki, C. Sutton, H. Emoto, H. Kambic, and J. Hollman. Effects of stent design and serum cholesterol level on the restenosis rate in atherosclerotic rabbits. *Am. Heart J.* 128:1049–1058, 1993.
16. Viñuela, F. North American experience in the embolization of intracranial aneurysms with GDC system. American Society of Neuroradiology, 30th Annual Meeting, St. Louis, MO, May 31–June 6, 1992.
17. Wakhloo, A. K., F. Schellhammer, J. de Vries, J. Haberstroh, and M. Schumacher. Self-expanding and balloon-expandable stents in the treatment of carotid aneurysms: an experimental study in a canine model. *Am. J. Neuroradiol.* 15:493–502, 1994.
18. Wakhloo, A. K., F. O. Tio, B. B. Lieber, F. Schellhammer, M. Graf, and L. N. Hopkins. Self expanding nitinol stents in canine vertebral arteries: hemodynamics and tissue response. *Am. J. Neuroradiol.* 16:1043–1051, 1995.
19. Weir, B. Aneurysms Affecting the Nervous System. Baltimore: Williams & Wilkins, 1987. pp. 1–60.
20. Whitmore, R. L. Rheology of the Circulation. Oxford: Pergamon Press, 1968, pp. 93–133.